AD-A074 369 NAVAL RESEARCH LAB WASHINGTON DC F/G 8/3
OCEAN WAVE SPECTROMETER MEASUREMENTS IN THE GULF STREAM EXPERIM--ETC(U)
AUG 79 D T CHEN, D L HAMMOND, P BEY

UNCLASSIFIED NRL-MR-4070 SBIE-AD-E000 321 NL

| OF |
AD
A074369

END
DATE
FILMED
10-79
DDC

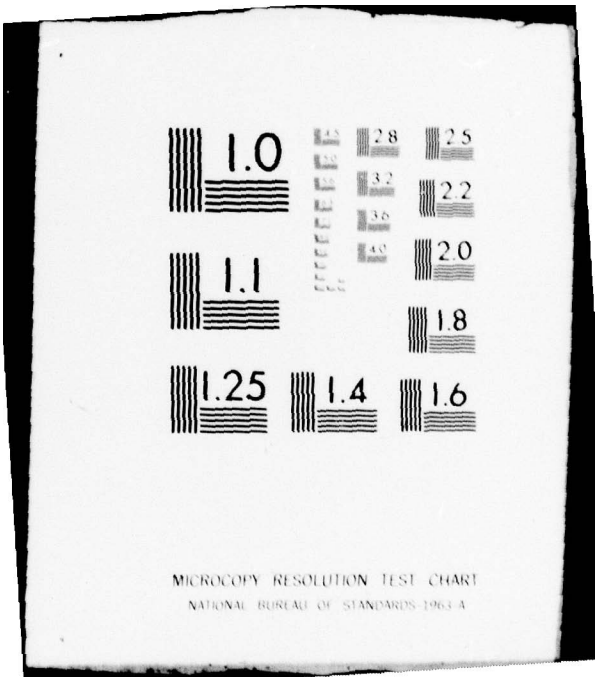
1.0
1.1
1.25
1.4
1.6
2.8
3.2
3.6
4.0
2.5
2.2
2.0
1.8
MICROCOPY RESOLUTION TEST CHART
NATIONAL BUREAU OF STANDARDS-1963-A

(12) LEVEL III

NRL Memorandum Report 4070

(6) # Ocean Wave Spectrometer Measurements in the Gulf Stream Experiment.

(10) DAVIDSON T. CHEN, DONALD L. HAMMOND, AND PAUL BEY

Advanced Space Sensing Applications Branch
Space Science Division

(11) 20 Aug 79

(12) 54p.

(14) NRL-MR-4070

August 20, 1979

(9) Final rept.,

(18) SBIE

(19) AD-E000 321

(16) F52553; RR03103

(17) WF52553000; RR031 0343

NAVAL RESEARCH LABORATORY
Washington, D.C.

JOB

251 950

SECURITY CLASSIFICATION OF THIS PAGE (When Data Entered)

REPORT DOCUMENTATION PAGE

READ INSTRUCTIONS BEFORE COMPLETING FORM

1. REPORT NUMBER: NRL Memorandum Report 4070
2. GOVT ACCESSION NO.:
3. RECIPIENT'S CATALOG NUMBER:

4. TITLE (and Subtitle): OCEAN WAVE SPECTROMETER MEASUREMENTS IN THE GULF STREAM EXPERIMENT
5. TYPE OF REPORT & PERIOD COVERED: Final Report on one phase of task.
6. PERFORMING ORG. REPORT NUMBER:

7. AUTHOR(s): Davidson T. Chen, Donald L. Hammond and Paul Bey
8. CONTRACT OR GRANT NUMBER(s):

9. PERFORMING ORGANIZATION NAME AND ADDRESS: Naval Research Laboratory, Washington, DC 20375
10. PROGRAM ELEMENT, PROJECT, TASK AREA & WORK UNIT NUMBERS: NRL Problem G01-10, Project WF52-553-000 (Continues)

11. CONTROLLING OFFICE NAME AND ADDRESS:
12. REPORT DATE: August 20, 1979
13. NUMBER OF PAGES: 53

14. MONITORING AGENCY NAME & ADDRESS(if different from Controlling Office):
15. SECURITY CLASS. (of this report): UNCLASSIFIED
15a. DECLASSIFICATION/DOWNGRADING SCHEDULE:

16. DISTRIBUTION STATEMENT (of this Report)

Approved for public release; distribution unlimited.

17. DISTRIBUTION STATEMENT (of the abstract entered in Block 20, if different from Report)

18. SUPPLEMENTARY NOTES

19. KEY WORDS (Continue on reverse side if necessary and identify by block number)

Ocean wave spectrometer
Directional wave slope spectra
Gulf Stream Experiment
Specular point model

20. ABSTRACT (Continue on reverse side if necessary and identify by block number)

By assuming finite conducting, Gaussian-distributed, statistically stationary and homogeneous ocean surface, the ocean wave spectrometer measurements made in the Gulf Stream Experiment have demonstrated the capability of inferring the directional wave number slope spectra by using the specular point model for look-angles of less than 20°. These measurements have also demonstrated the necessity of independent measurements of wind direction, mean square surface slope,

(Continues)

DD FORM 1 JAN 73 1473 EDITION OF 1 NOV 65 IS OBSOLETE
S/N 0102-014-6601

SECURITY CLASSIFICATION OF THIS PAGE (When Data Entered)

10. Program Element, Project, Task Area & Work Unit Numbers (Continued)

NRL Problem G01-10E
Project RR-031-03-43

20. Abstract (Continued)

and foam and spray. The results also indicate that at least four independent directional measurements with spatial resolution of 0.1 meters or smaller and spatial coverage of 750 to 1000 meters are necessary.

CONTENTS

OCEAN WAVE SPECTROMETER MEASUREMENTS IN THE GULF STREAM EXPERIMENT

I. INTRODUCTION

Interests in ocean wave-measuring space-borne instruments have increased steadily in recent years with the recognition of their potential for providing synoptic measurements continuously and globally. The scientific and economic benefits from such measurements are multi-disciplined as well as inter-disciplined. These benefits include, for example, the better understanding of ocean dynamics and air-sea interactions so that reliable, well-conceived, and proven physical and mathematical models can be developed for the long and the short range predictions of currents, tides, sea state, coastal processes, etc. These benefits also include those tangible benefits for the Navy as defined by Chen (1978) and for the general public as reported by "SEASAT-A Scientific Contribution" (1974).

Many sensors which show promise for remote sensing of ocean surface parameters are active microwave devices. These microwave remote sensors operate in the domain of frequencies in which the electromagnetic waves will penetrate cloud cover, interact with waves, and yet are independent of solar ambient radiation. These characteristics are very desirable and appropriate for remote sensors which monitor ocean surface structures.

Among the many sensors being investigated is the Naval Research Laboratory's (NRL's) airborne X-band

Note: Manuscript submitted July 2, 1979.

nanosecond wave spectrometer. This NRL X-band wave spectrometer was designed originally to be used as an altimeter, and is operated at 9.75 GHz with a pulse-repetition frequency of 90 KHz and may also be operated with a variable pulse width (Yaplee, et al, 1971; Walsh, 1974). Pulses are 2 ns long and the horns have a beam-width of 5^{o}. The wave spectrometer records the signal scattered from a single transmitted pulse by sampling from a sequence of transmitted pulses with samples taken at progressively later times. In other words, the first transmitted pulse is sampled at time t_1, and the next transmitted pulse is sampled at a time after t_1 at the preset time interval, and so forth, until 160 samples have been recorded as shown in Figure 1.1. These 160 samples constitute a complete wave spectrometer sweep which is recorded on the digital tape after Analog to Digital conversion. It requires 1/90 second to complete one sampling procedure.

It is very important, however, to observe that, due to the particular data acquisition procedures, the wave spectrometer has relatively strong signal returns. This feature is the major difference between NRL's wave spectrometer and that of the Goddard Space Flight Center (GSFC) of the National Aeronautics and Space Administration (NASA) as described by Le Vine, et al (1977a).

The horns are mounted on a movable platform with a port under the belly of the aircraft for pointing the horns off the right side of the aircraft at 15^{o} off nadir. The wave spectrometer is usually flown at an altitude of 1500 meters. This altitude is high enough for neglecting the effects due to the aircraft motions but yet is low enough for providing adequate spatial resolution for the measurements. One site measurement usually consisted of several

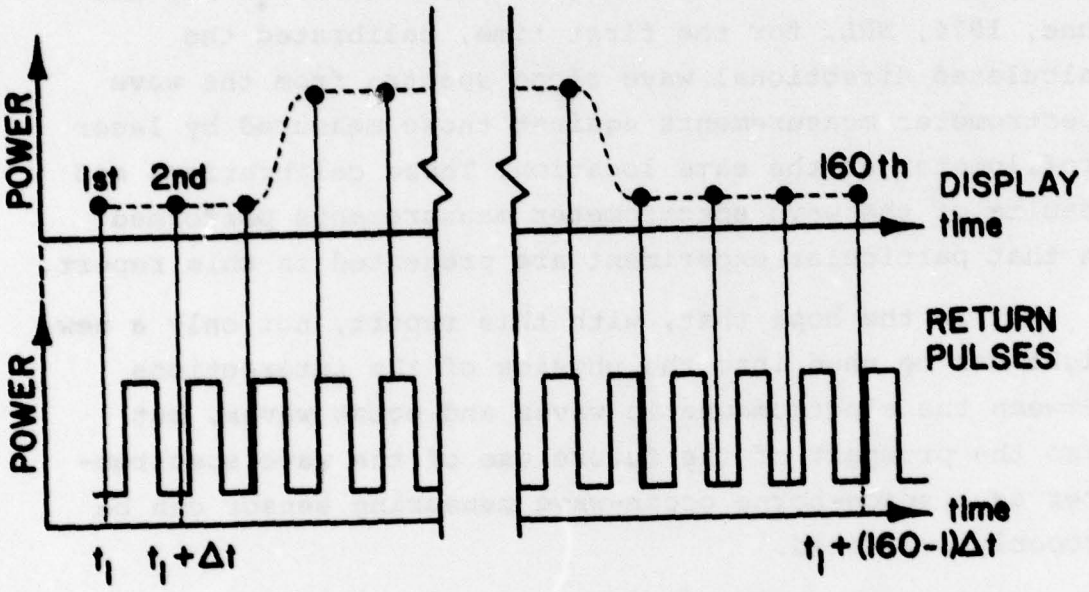

Δt: preset time interval

Fig. 1.1 - Displaying return pulses by means of the sampling technique

straight flight lines in various directions with respect to the wind.

The results, in the form of the directional wave slope spectra, are calculated. In the Gulf Stream Experiment (McClain, et al, 1978) conducted jointly by NRL and NASA's Wallops Flight Center (WFC) in May and June, 1976, NRL, for the first time, calibrated the calculated directional wave slope spectra from the wave spectrometer measurements against those measured by laser profilometer at the same location. These calibrations and results of the wave spectrometer measurements performed in that particular experiment are presented in this report.

It is the hope that, with this report, not only a new light can be shed into the physics of the interactions between the electromagnetic waves and ocean waves, but also the prospect of the future use of the wave spectrometer as a space-borne ocean-wave measuring sensor can be properly evaluated.

II. OCEAN WAVE SPECTROMETER

The fundamental concept of obtaining directional ocean wave spectra by short pulse radar from space was first suggested by Tomiyasu (1971). He proposed that the directional ocean wave spectra could be related to modulation of the range-time display of the radar. He suggested also the uses of 10 ns pulses and a spectral analyzer as the signal processer for satellite application. However, he was not very specific on the scattering mechanism involved. Although he did not use the word "directional", it was well-understood to be such.

Subsequently NRL converted and modified the existing nanosecond radar, which was used primarily as a radar altimeter (Yaplee, et al, 1971; Walsh, 1974), to be used

as the directional ocean wave measuring sensor called the wave spectrometer. NRL performed its first wave spectrometer experiment in the Joint North Sea Experiment - 73 (JONSWAP-73) as reported by Eckerman and Hammond (1974). In those flights, the wave spectrometer was mounted in nadir position in the belly of the NASA WFC C-54. To obtain data with the beam pointing at angles off nadir, the aircraft was put into banking turns. Data were obtained in this manner at angles of 10° and 15° with the aircraft at an altitude of 3000 meters. As the result of these banking turns, the direction of the beam was continuously changing with respect to the wind direction, and there were also some uncertainties in the pointing angle. During these experiments NASA Langley Research Center's (LRC's) laser profilometer on board malfunctioned; therefore, the ground truth on wave structure which was supposed to be provided by this laser profilometer was not obtainable. Nevertheless, the limited experiment had demonstrated successfully the concept of a wave spectrometer.

GSFC, inspired by this initial success, decided to convert the GEOS-3 (Geodetic Earth-Orbiting Satellite 3) breadboard Ku-band radar altimeter into a wave spectrometer with a look-angle of 30° (Le Vine, et al, 1977a and 1977b). NRL also improved the original wave spectrometer system not only by installing movable horns mounted at 15° off nadir but also by developing continuously the software programs and data analysis techniques. In the mean time NRL scientists had successfully improved the laser profilometer software programs so that reliable ocean wave spectra could be derived (McClain, et al, 1978). In May and June, 1976, the joint NRL and NASA/WFC Gulf Stream Experiment offered the first reasonable opportunity to calibrate the wave

spectrometer measurements against those by the laser profilometer.

The fundamental concept of obtaining ocean wave structure contains two important parts. The first part of the concept is that one is able to determine or resolve the physical distance along the surface of the ocean, with confidence, from the slant angle of the pulse return. Let this part be called the Ability to Resolve Spatially. The second part of the concept is that the return power is proportional to local wave slope, or the slope of local wave facet as defined by Schooley (1962), normal to the wave spectrometer incident angle. Similarly, this part can be called the Ability to Resolve the Local Wave Slope.

The ability to resolve spatially is directly associated with wave number, k, which is defined as $2\pi/L$ and L is the wave length. And the ability to resolve the local wave slope is associated with the term, ak, where a is the wave amplitude. This term of ak is the perturbation parameter in the nonlinear wave analysis of physical mechanisms such as wave-wave interactions. It is quite obvious that the wave amplitude a can be inferred if both the wave number, k, and the wave slope amplitude, ak, are known. And it is also easy to see that this inferred wave amplitude is independent of the error associated with the wave number.

Discussions of both of these Abilities and their backgrounds, and derivations are going to be presented separately in the following sections:

1. Ability to Resolve Spatially.

This concept can be illustrated the best with the aid of figures. Figure 2.1(a) shows the horns, of the wave spectrometer, mounted under the belly of the aircraft which is flying into the figure with the speed of v. The horns

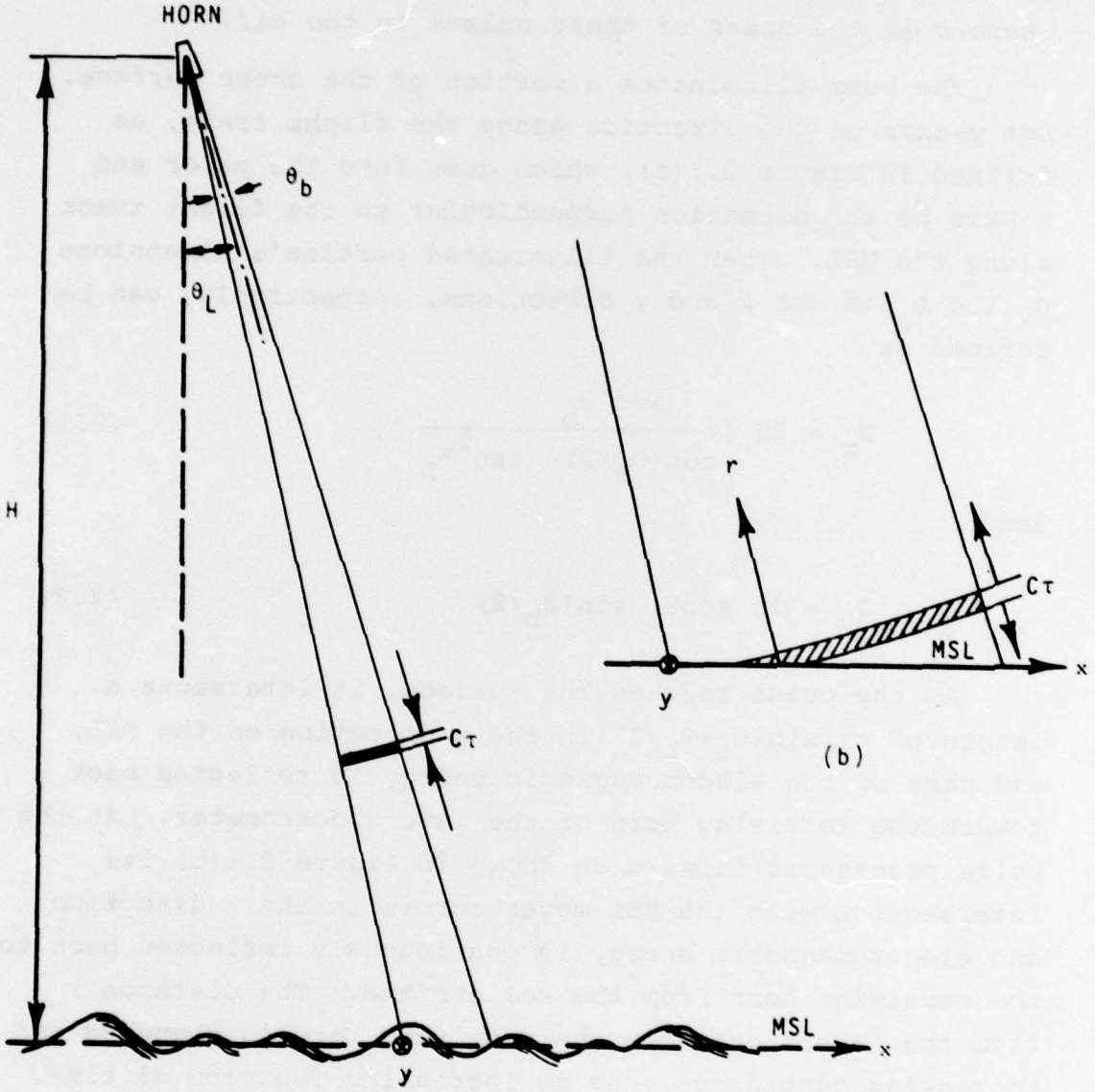

Fig. 2.1 - Physical configurations

are kept at an altitude of H above the mean sea level (MSL), and have look-angle Θ_L off the nadir. The wave spectrometer radiates a series of compressed short pulses with duration τ to the ocean surface from the transmitting horn whose beamwidth is Θ_b. These pulses have spatial width of $c\tau$ where c is the speed of these pulses in the air.

The beam illuminates a portion of the ocean surface. Let y-axis be the direction along the flight track, as defined in Figure 2.1(a), which goes into the paper and x-axis be the direction perpendicular to the flight track along the MSL. Then the illuminated portion's dimensions D_x and D_y in the x and y directions, respectively, can be defined as

$$D_x = 2H \left[\frac{\sec^2\Theta_L}{\cot(\Theta_b/2) - \tan^2\Theta_L}\right], \qquad (2.1)$$

and

$$D_y = 2H \sec\Theta_L \sin(\Theta_b/2). \qquad (2.2)$$

As the pulse reaches the surface, it intersects a length of $c\tau/\sin(\Theta_L-\Theta_b/2)$ in the x direction on the MSL, and part of the electromagnetic energy is reflected back toward the receiving horn of the wave spectrometer. As the pulse propagates forward as shown in Figure 2.1(b) its intersection with the MSL moves across in the x direction and electromagnetic energy is continuously reflected back to the receiving horn from the sea surface. The distance r from the intersection to the receiving horn is changing and increasing continuously as an increasing function of time. Therefore, by simple geometry, the recording of the arrival time t of the reflected pulse can be related to the instantaneous footprint which is the illuminated portion of the ocean surface.

Figure 2.2 shows this geometric relationship where x_o is the location of the y-axis off nadir on the x-axis at time t_o. At time t the position of this intersection is at (x, vt). However, the term vt is more or less zero because t is a quantity of nanoseconds and v is approximately in order of 100 meters per second for the aircraft. The position of the intersection at time t in this case can simply be approximated as (x,0). In other words, the intersections can be assumed to be propagating along the x-axis only. Therefore, the returned electromagnetic energy has to make an angle of θ to the nadir and a distance r to the receiving horn. From Pythagorean Theorem,

$$r^2 = H^2 + (x_o+x)^2 , \tag{2.3}$$

and

$$r_o^2 = H^2 + x_o^2 . \tag{2.4}$$

Equation (2.3) can be redefined as

$$(r_o + \delta r)^2 = H^2 + (x_o + x)^2 . \tag{2.5}$$

where δr is the increment of r, also called range, over the original range r_o at time t_o. By Equations (2.3), and (2.5)

$$\delta r = [(x_o + x)^2 + H^2]^{1/2} - r_o . \tag{2.6}$$

Since the incremented range δr is recorded discretely with respect to time, it is necessary to resolve the corresponding x by the following substitutions,

$$\delta r = n \, \Delta r, \tag{2.7}$$

and

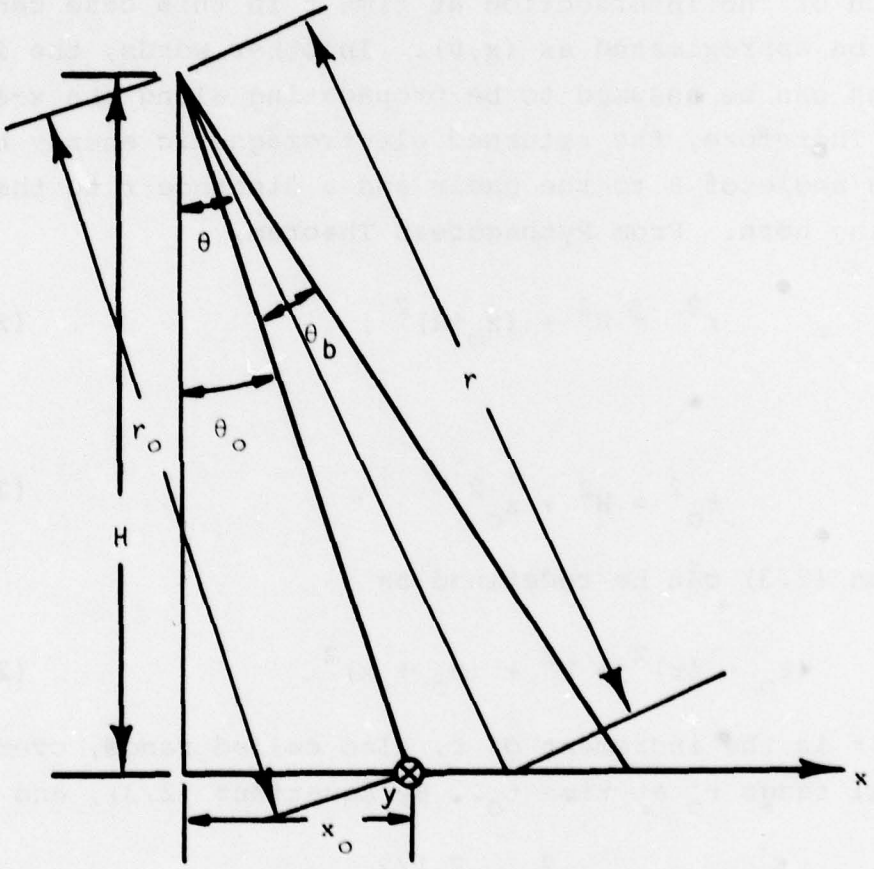

Fig. 2.2 - Geometry

$$x = m\,\Delta x \tag{2.8}$$

where Δx can be defined as the required spatial resolution along the ocean surface and Δr is the necessary range resolution from which the ocean surface spatial resolution Δx can be attained. As the consequence, Equation (2.6) can be restated as

$$n = \left[\left(m\,\frac{\Delta x}{\Delta r} + \frac{x_o}{\Delta r}\right)^2 + \left(\frac{H}{\Delta r}\right)^2\right]^{1/2} - \frac{r_o}{\Delta r} \tag{2.9}$$

where

$$x_o = H\,\sec\theta_o$$

$$= H\,\sec(\theta_L - \theta_b/2) \tag{2.10}$$

and θ_o is the initial value of θ at time t_o. It is quite obvious that m is an integer and n is a real number. The wave spectrometer must record the return pulses in an equally spaced and discrete manner, according to Equation (2.9), in order to generate an equal and discrete spatial resolution on the ocean surface.

By using Equation (2.9) with known H, θ_L, θ_b, Δx, and Δr the required values of n for the monotonically increasing m can be calculated. Since the range resolution Δr is related to the detection time interval Δt as

$$\Delta r = \frac{c\,\Delta t}{2}\ , \tag{2.11}$$

the position of the intersection, x, on the ocean surface is uniquely determined by the recorded time sequence of the return pulse. The spatial resolution Δx is determined by the range resolution Δr, or the detection time interval Δt, uniquely. This type of kinematic relationship enables the wave spectrometer the ability to resolve spatially.

2. Ability to Resolve the Local Wave Slope

The use of a short pulse radar to measure the ocean wave structure had been tried a couple of decades ago. One of the problems always has been the interpretation of the return signals such as radar cross sections, envelope of the return power, etc., in terms of the physical parameters of the ocean wave measured. Brooks and Dooley (1971) pointed out some constraints on the interpretations of this type as:

(1) the pulse spatial width, $c\tau$, projected on the ocean surfaces should be smaller than the shortest wave length of interest,

(2) wave-front curvature in the footprint on the ocean surface limits the smallest usable nadir angle, $\theta_L - \theta_b/2$; and

(3) the shortest resolvable wave is a function of the modulation index of the received signal, the signal bandwidth, and the pulse bandwidth.

In 1958, Myers (1958), using a X-band radar mounted on a tower, demonstrated a temporal correlation between wave-staff measurements and the modulation of power scattered back to the receiver. This work was done at incident angles near grazing. Zamarayev and Kalmaykov (1969) supported a similar observation at large incident angles also near grazing. Another X-band radar system with an extremely short pulse length of 1 ns and a nadir-pointed antenna beam has been used to measure wave profiles, and excellent correlation with wave staff measurements has been demonstrated by Yaplee, et al (1971). Their unpublished results also show excellent correlations at the incident angles of 15°, 30° and 45°.

Categorically, the correlations studied can be classified into two distinct types. The first kind,

represented by Myers (1958), showed the correlations between the radar cross section, or the intensity of the returned radar signal, and the wave amplitude or slope. The other kind, represented by Yaplee, et al (1971), exhibited the correlation between the radar range and the wave amplitude. Both types of correlations are functions of scattering between the electromagnetic waves and the ocean surface waves. Because of the special requirements for space applications, it is the intention of this report to concentrate on the first kind of correlations which is a strong function of scattering processes involved in the interactions between the electromagnetic waves and the ocean surface waves.

In their report, Brown and Miller (1977) had studied the microwave backscattering theory from the statistically stationary and homogeneous ocean surface for the active microwave sensors. Based upon the absolute order of magnitudes involved in the physical processes they took three approaches to formulate the mathematical problems. The first approach, called the boundary perturbation approach, is valid for

$$|\zeta| << \lambda, \tag{2.12}$$

and

$$|\nabla\zeta| << 1, \tag{2.13}$$

where ζ is the ocean surface profile, $\nabla\zeta$ is the slope of the ocean surface and λ is the wave length of the electromagnetic waves. This approach gives rise to a low frequency solution for rough surface scattering. Thus, except for near calm surface conditions. Equations (2.12) and (2.13) cannot be truly satisfied for the microwave frequencies above 1 GHz. Their second approach, called the

physical optical approach, is valid for

$$\rho >> \lambda \ , \tag{2.14}$$

$$|\nabla \zeta| < 1 \ , \tag{2.15}$$

and

$$(\overline{\zeta^2})^{1/2} \cos\theta >> \lambda \tag{2.16}$$

where ρ is the radius of curvature at every point of the ocean surface, overbar means ensemble average, and θ is the angle of incidence relative to the normal to the mean flat surface. This approach yields exact solutions for $\lambda \to 0$ and approximate solutions for $\lambda > 0$. The third approach, called the composite surface scattering approach, is simply the combination of the first two approaches.

It would appear for microwave frequencies, that scattering from the ocean surface can be analyzed using the physical optics approach since the root mean square (rms) amplitude of the waves are usually large. However, this is not borne out by observations. Although the characteristics of the ocean surface satisfy Equations (2.15) and (2.16), they do not always satisfy Equation (2.14). On the other hand, the boundary perturbation approach cannot be valid if the microwave frequency exceeds 1 GHz. And, usually, the characteristics of the ocean surface cannot always satisfy Equation (2.13).

Based upon his observation of small wave amplitude short wave length waves riding on the larger wave amplitude longer wave length waves, Wright (1968) presents the argument for his composite scattering approach. This approach was so-named because of the incoherent addition of the large-scale-dependent physical optics result with

the tilted-plane Bragg scattering solution.

Taking the first order approach, for a random, finitely conducting and Gaussian ocean surface, Barrick (1968) proposes the specular point model which evaluates the radar cross section σ_o per unit area to be

$$\sigma_o = \frac{\sec^4\theta}{\overline{(\nabla\zeta)^2}} \exp(-\tan^2\theta / \overline{(\nabla\zeta)^2}) \; |R(0)|^2 \qquad (2.17)$$

where overbar means ensemble average, θ is the incident angle of the electromagnetic wave ray to the normal of the mean sea level, and R(0) is the Fresnel reflection coefficient of the space-to-surface interface for normal incidence or $\theta=0^o$. A relationship between the averaged mean square surface slope, $\overline{(\nabla\zeta)^2}$, and average wind speed, U, has been given empirically by Cox and Munk (1954) as

$$\overline{(\nabla\zeta)^2} = 0.003+0.00512U \qquad (2.18)$$

where U is measured in meters per second at 12.5 meters above the mean sea level. Nevertheless, it is desirable to have $\overline{(\nabla\zeta)^2}$ measured independently. The justification for the independent measurement of $\overline{(\nabla\zeta)^2}$ can be found in Section 6. Equation (2.17) has good agreement with the work of others, in particular that of Hagfors (1964). Since the ocean wave spectrometer is operated with look-angles less than 20^o from the nadir with all the required assumptions satisfied, it is desired to use Equation (2.17) as the mathematical model to resolve the local wave slope.

It is quite important to notice that, from Equation (2.17), the angle θ can be evaluated from known quantities of σ_o, $\overline{(\nabla\zeta)^2}$, and R(0). $\overline{(\nabla\zeta)^2}$ can be obtained by Equation (2.18) if the average wind speed U is measured simultaneously.

It is also very important to bear in mind that Equation (2.17) is the result of long duration of observation or measurement. The angle θ, thus derived, is indeed the incident angle of the electromagnetic wave ray to the normal of the mean sea surface as shown in Figure 2.2. However, for the instantaneous measurement of σ_o as a function of time, the angle inferred should be $\theta-\kappa$ where κ is related to the local wave slope. In other words,

$$\overline{\theta-\kappa} = \theta \tag{2.19}$$

where θ can be inferred, independently, also from the time sequence of the radar return. The relationship between the angle κ, thus, obtained and the local wave slope can be established by geometry as

$$O(ak) = \tan\kappa \tag{2.20}$$

where O(ak) means Order of ak.

Therefore, by using Equations (2.17), (2.18), (2.19), and (2.20) and also the spatial resolving ability of the wave spectrometer the local wave slope can be determined. Since R(0) may be assumed to be constant, its absolute value is irrelevant in the numerical manipulation.

Nevertheless, the return radar signal received by the horn is power which is dependent on system characteristics and target characteristics. Ignoring the effects of the intervening medium, for a target such as the sea surface, the return power P_r can be expressed in terms of transmitted power P, the antenna gain G, the operating wave length λ, the range to the target r, and the scattering cross section per unit area σ_o (Skolnik, 1970) as

$$P_r = \frac{\lambda^2}{(4\pi)^3}\int_A \frac{PG^2\sigma_o}{r^4}\, dA \tag{2.21}$$

where A is the illuminated area. By knowing P, G, A, and λ the scattering radar cross section per unit area σ_o can be obtained from the measured P_r and inferred r. The radar cross section σ_o so calculated can be used directly in Equations (2.17), (2.18), (2.19), and (2.20) with the known mean wind speed U or mean square surface slope $\overline{(\nabla\zeta)^2}$ for the evaluation of the local wave slope. Therefore, Equations (2.17) to (2.21) define the ability to resolve local wave slope by the wave spectrometer.

III. DATA ANALYSIS

Figure 3.1 shows one of the return pulses. The vertical axis shows the return radar signal in the unit of milivolts. And the horizontal axis is the time in unit of nanoseconds. Experimentally, the time axis can be changed at will by a dial setting in accordance with the spatial resolution requirements. The return pulse is recorded at 160 points, or gates. In the particular example shown by Figure 3.1 the time interval between two successive gates is chosen to be 20 ns. The total time span for the complete pulse is 3180 ns.

Each data record consists of 256 pulses at 90 Hz, and 32 records make one file. The mean of one record, which is the "antenna pattern", is shown in Figure 3.2. By Equation (2.11) the horizontal axis has been converted from time to range in meters. The effects of this antenna pattern on the return pulses are subsequently removed.

By the registered time sequence n as shown in Equation (2.7), with the preset known time interval Δt and known distance increment Δx the integer m can readily evaluated from Equations (2.4), (2.8), (2.10), (2.11), and (2.9). As the consequence, x is known by Equation (2.8). Referring back to Figure 2.2 the angle θ is known once x, x_o and H

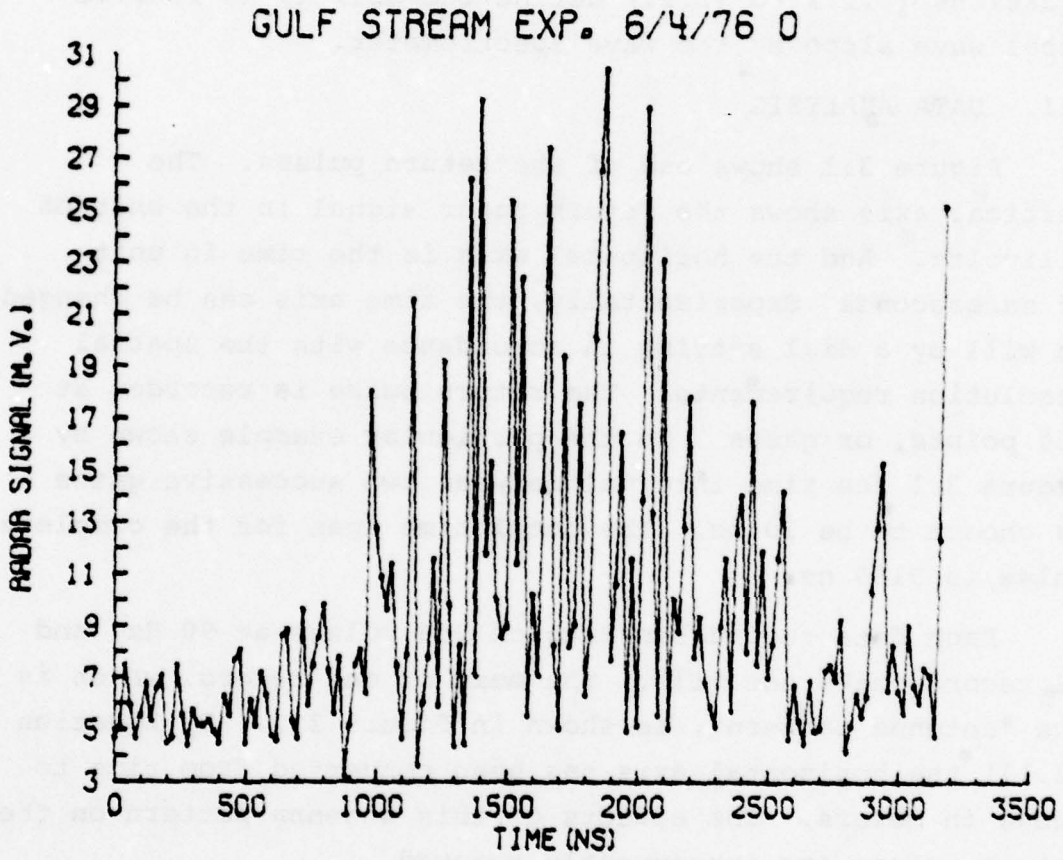

Fig. 3.1 - Return pulse

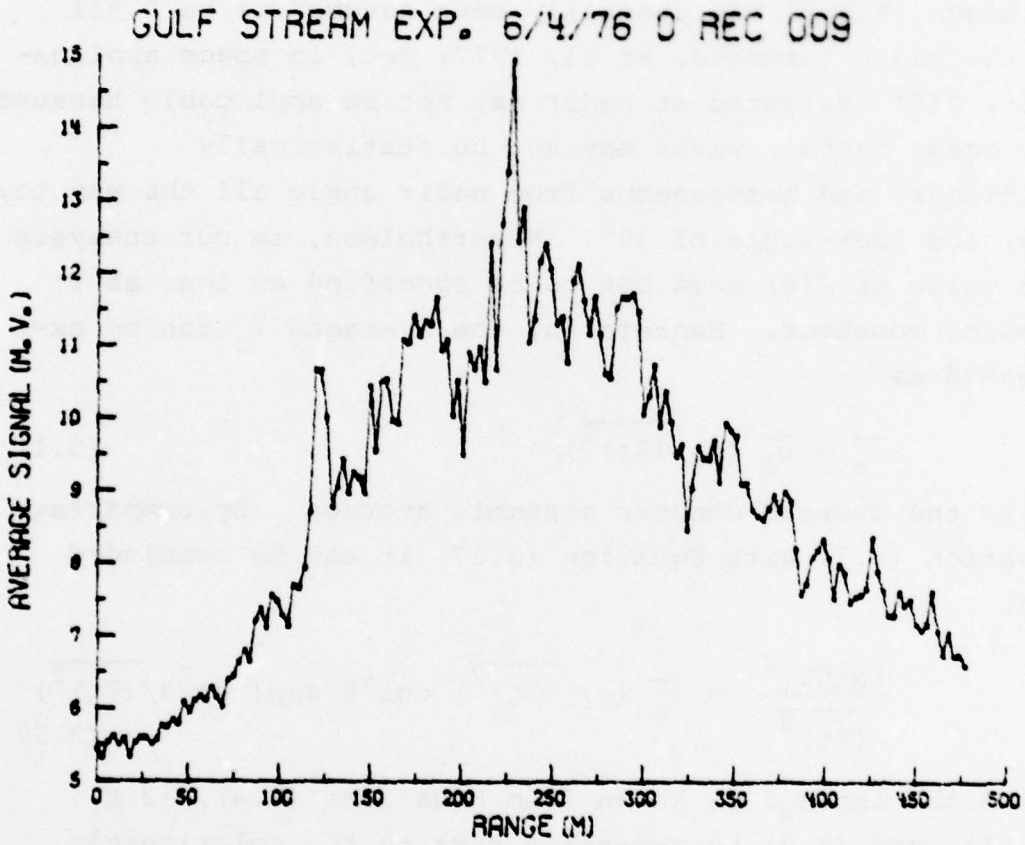

Fig. 3.2 - Antenna pattern

are all evaluated.

Summing up all the radar cross section per unit area σ_o for every look-angle θ by using Equation (2.21) the averaged value of σ_o should satisfy Equation (2.17). However, the value of R(0) in Equation (2.17), the Fresnel reflection coefficient of the space-to-surface interface for normal incidence or $\theta = 0^o$, is rather difficult to measure unless the value of $\overline{(\nabla\zeta)^2}$ at $\theta = 0^o$ is also known. Although $|R(0)|^2$ has generally been assumed to be 0.631 at the nadir (Hammond, et al, 1977) yet, in space application, R(0) evaluated at nadir may not be applicable because the ocean surface waves may not be statistically stationary and homogeneous from nadir angle all the way to, say, the look-angle of 30^o. Nevertheless, in our analysis the value of R(0) need not to be specified as long as it remains constant. Henceforth, the averaged $\overline{\sigma_o}$ can be expressed as

$$\overline{\sigma_o} = \overline{\sigma_o}\ (\theta,\ \overline{(\nabla\zeta)^2}) \tag{3.1}$$

where the overbar denotes ensemble average. By comparing Equation (3.1) with Equation (2.17) it can be concluded that

$$\frac{|R(0)|^2}{\overline{(\nabla\zeta)^2}} = \overline{\sigma_o}\ (\theta,\ \overline{(\nabla\zeta)^2})\ \cos^4\theta\ \exp(\tan^2\theta/\overline{(\nabla\zeta)^2}) \tag{3.2}$$

where the angle θ is known from Equations (2.4), (2.8), (2.11), and (2.9) by referring back to the relationship shown by Figure 2.2. The mean square surface slope $\overline{(\nabla\zeta)^2}$ in Equation (3.2) is desired to be measured independently as has been done in this experiment. Otherwise, Equation (2.18) can be used as alternative means to evaluate $\overline{(\nabla\zeta)^2}$ if the mean wind U is known. If Equation (2.18) is

used for the evaluation of $\overline{(\nabla\zeta)^2}$, a different set of calibrations is required, for reasons which will be given in the following sections.

For each angle θ the individually measured $\sigma_o(\theta, \xi)$ satisfies

$$\frac{\sigma_o(\theta, \xi)}{\overline{\sigma_o}} = \sec^4\xi \exp(-\tan^2\xi/\overline{(\nabla\zeta)^2}) \qquad (3.3)$$

with respect to Equations (2.17) and (3.2). The angle ξ, by using Equation (2.19), is defined as

$$\kappa = \theta - \xi \qquad (3.4)$$

where κ is the local tangent angle of the ocean wave and should satisfy Equation (2.20).

As it turns out this alternative approach represented by Equations (3.1) to (3.4) can circumvent the difficult task of evaluating R(0) and, yet, a meaningful correlation relationship can still be established between the radar cross section per unit and the local wave slope.

Figure 3.3 shows the local wave slope derived from one return pulse. The horizontal axis has been further converted, by using Equations (2.3) to (2.11), to the distance along the ocean surface in meters.

Subsequently, prewhitening filtering as recommended by Blackman and Tukey (1958) is applied to the data. This step is necessary for two reasons. The first reason is to remove segments of components whose wave lengths are longer than those inferred by the data segment. The second reason is to decrease the side lobes of the transform that are introduced by analyzing data intervals of finite length.

The directional wave number slope spectra, as shown in Figure 3.4, are evaluated for each file by using the Fast

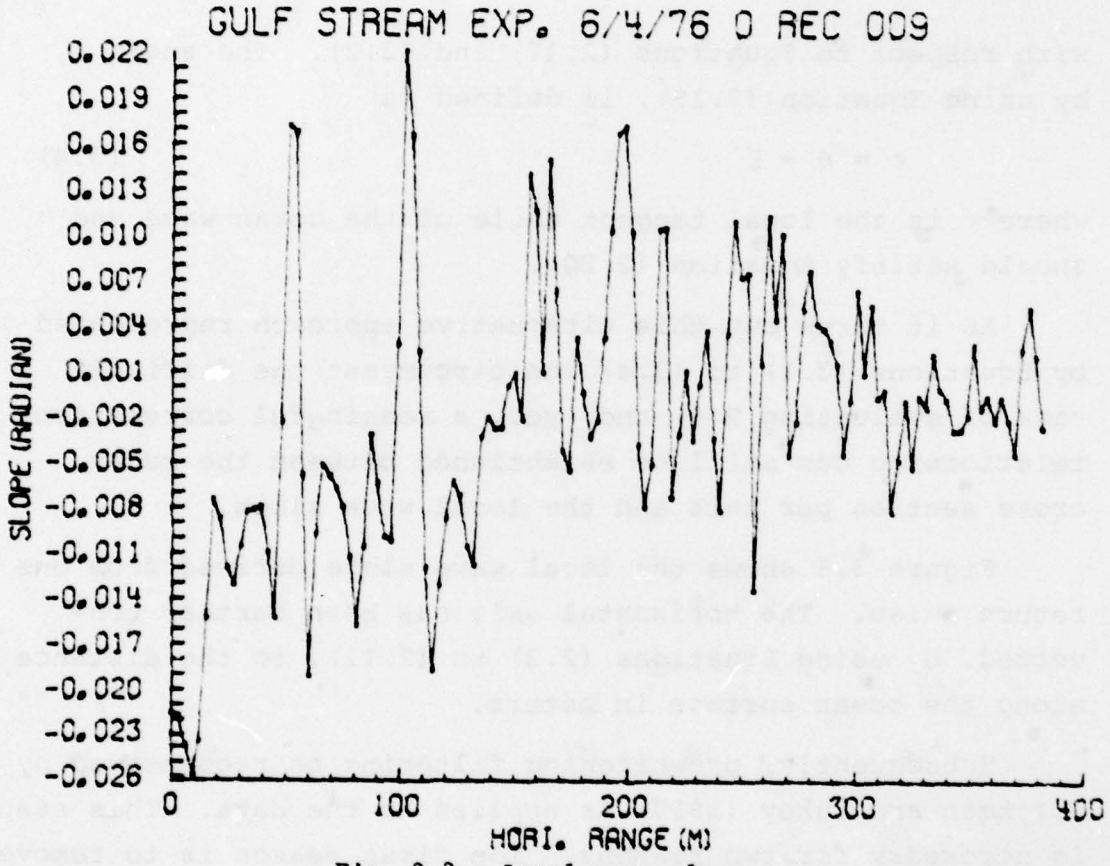

Fig. 3.3 - Local wave slope

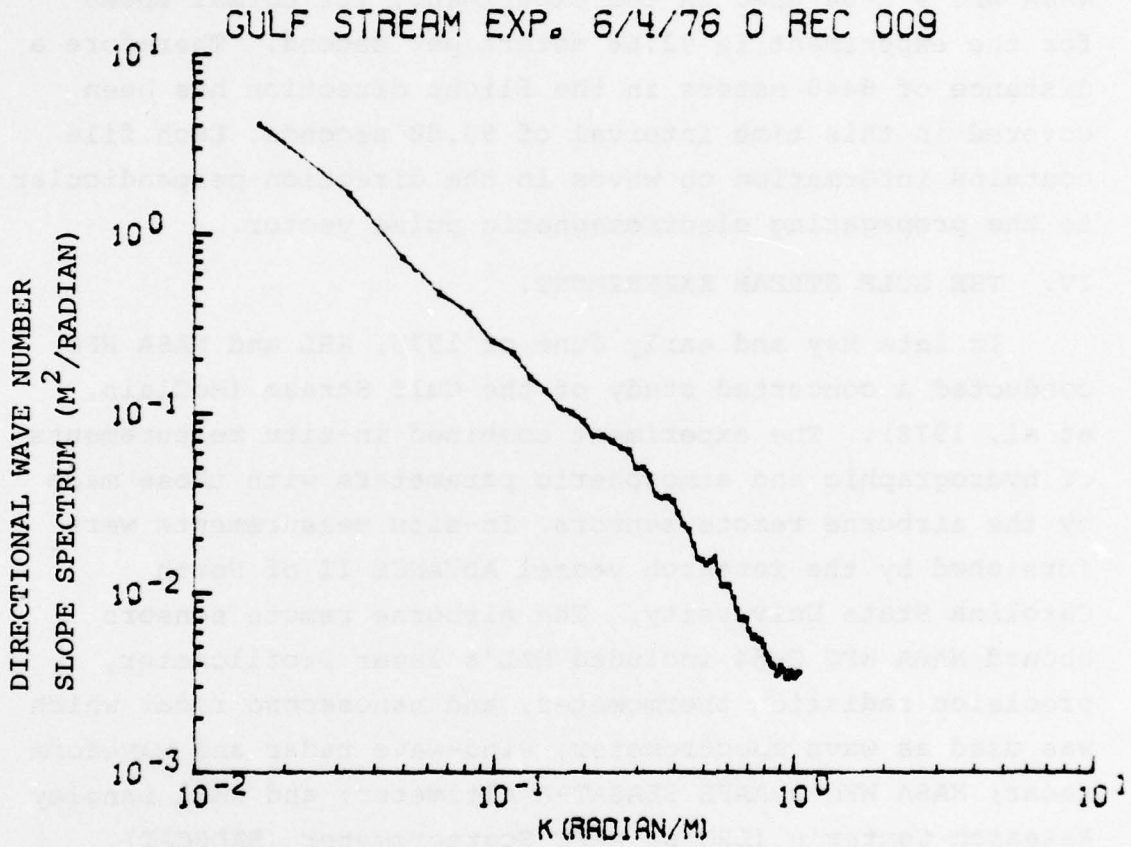

Fig. 3.4 - Directional wave number slope spectrum

Fourier Transform and the Hanning filter (Blackman and Tukey, 1958) on tanκ where κ is given by Equation (3.4). The horizontal axis is the wave number, k, in the unit of radian per meter and both axes are in logarithmic scale.

Each file of 32 records of 256 return pulses takes slightly over 90.88 seconds for recording while the aircraft is flying at v meters per second. In the case of NASA WFC's C-54 used in the experiment, its normal speed for the experiment is 92.66 meters per second. Therefore a distance of 8448 meters in the flight direction has been covered in this time interval of 90.88 seconds. Each file contains information on waves in the direction perpendicular to the propagating electromagnetic pulse vector.

IV. THE GULF STREAM EXPERIMENT.

In late May and early June of 1976, NRL and NASA WFC conducted a concerted study of the Gulf Stream (McClain, et al, 1978). The experiment combined in-situ measurements of hydrographic and atmospheric parameters with those made by the airborne remote sensors. In-situ measurements were furnished by the research vessel ADVANCE II of North Carolina State University. The airborne remote sensors aboard NASA WFC C-54 included NRL's laser profilometer, precision radiation thermometer, and nanosecond radar which was used as wave spectrometer, wind-wave radar and waveform radar; NASA WFC's AAFE SEASAT-A altimeter; and NASA Langley Research Center's (LRC's) AAFE Scatterometer (RADSCAT).

The research area was located due east of WFC covering both sides of the Gulf Stream western boundary. The experiment provided an excellent opportunity to calibrate wave spectrometer measurements against those provided by the laser profilometer. The wave spectrometer acquired data at the altitude of 1524 meters, with a star pattern as shown by Figure 4.1. Then the aircraft spiraled down to the

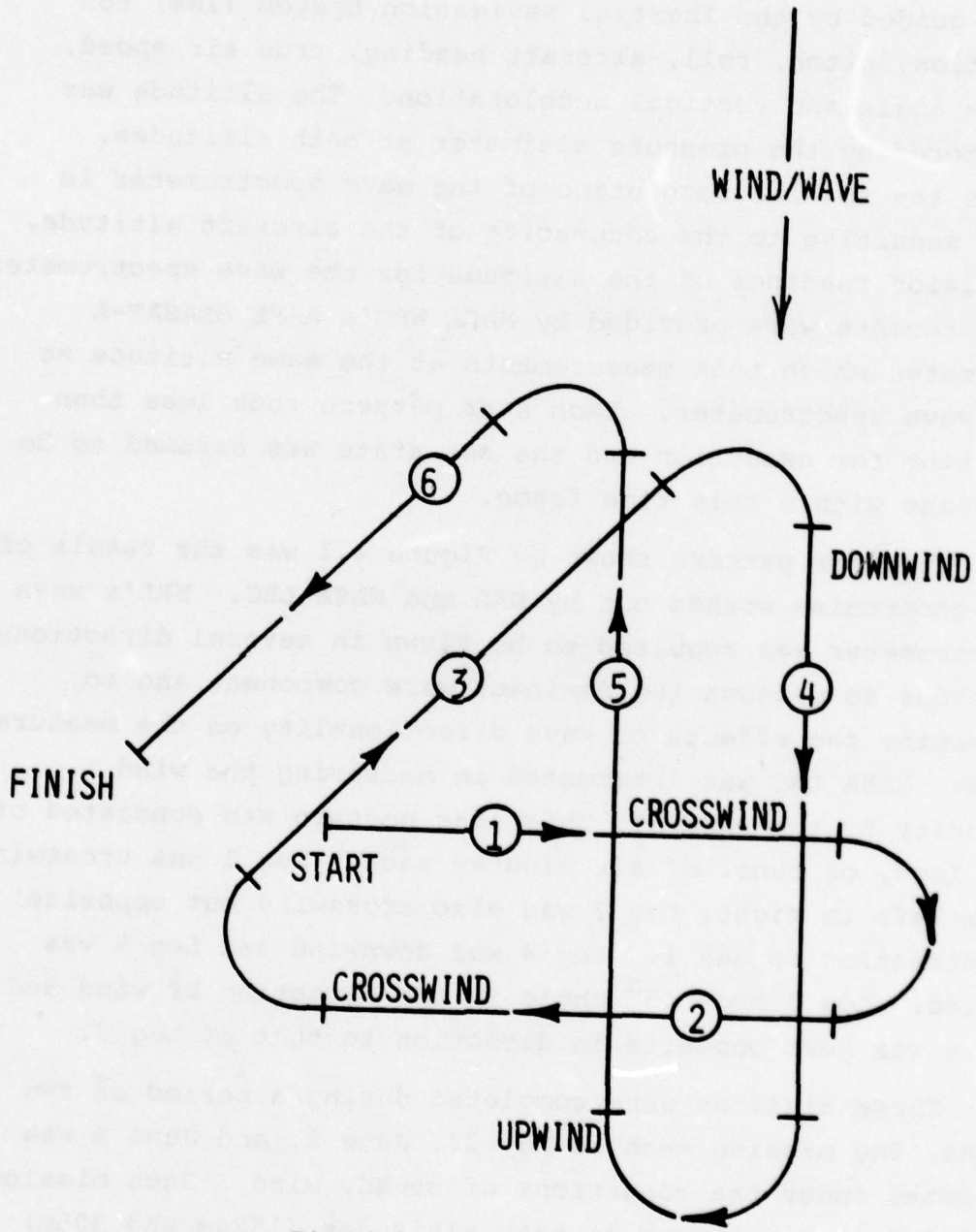

Fig. 4.1 - Star pattern

altitude of 305 meters and flew another star pattern for the laser profilometer measurements. These two different star patterns were flown over the same ocean area guided by the Inertial Navigation System (INS) for location, pitch, roll, aircraft heading, true air speed, track angle and vertical acceleration. The altitude was monitored by the pressure altimeter at both altitudes. Since the spatial resolution of the wave spectrometer is very sensitive to the accuracies of the aircraft altitude, precision readings of the altitude for the wave spectrometer measurements were provided by NASA WFC's AAFE SEASAT-A altimeter which took measurements at the same altitude as the wave spectrometer. Each star pattern took less than one hour for execution and the sea state was assumed to be constant within this time frame.

The star pattern shown by Figure 4.1 was the result of the compromise worked out by NRL and NASA LRC. NRL's wave spectrometer was required to be flown in several directions in order to measure the dominant wave component and to determine the effects of wave directionality on the measurement. NASA LRC was interested in measuring the wind velocity by the RADSCAT. This star pattern was consisted of six legs, or runs, of six minutes each. Leg 1 was crosswind from left to right, Leg 2 was also crosswind but opposite in direction to Leg 1. Leg 4 was downwind and Leg 5 was upwind. Leg 3 made 45^{o} angle to the direction of wind and Leg 6 was just opposite in direction to that of Leg 3.

Three missions were completed during a period of two weeks. One mission each on May 27, June 2, and June 4 was executed under the conditions of steady wind. Each mission included star patterns at both altitudes (1524m and 305m) flown over a location to the east of the Gulf Stream's western boundary and over another location to the west of

this boundary.

It was unfortunate that the INS malfunctioned for the first two missions so that wave spectra were unable to be evaluated with confidence from the laser profilometer measurements. The results presented were derived from the third mission conducted on June 4.

Hindcast indicated, on June 4, that a high pressure ridge extended in a East-West direction over the Great Lakes. This pressure pattern generated southwesterly wind through the experiment area. The wind speed was low, however. The ship ADVANCE II reported that the wind speed was 7.5 meters per second southwesterly on 4 June at 1:00 P.M. eastern daylight saving time.

The high sea state occurred on 4 June could not be totally attributed to wind-generated waves but was also a result of swells generated earlier that morning from somewhere else as well. ADVANCE II recorded that the dominant wave, swell in this case, had a constant direction at all stations with a heading of 225^{o} which was the same direction as the wind that morning.

Based on Figure VI-5b of the Gulf Stream Experiment report (McClain, et al, 1978) several oceanographic physical parameters can be computed readily from NRL airborne laser profilometer data and are tabulated in Table 4.1.

Table 4.1 Oceanographic Physical Parameters for June 4, 1976

Wave Number Slope Spectral Peak, $S(k_o)$	0.0442 meter.radian
Dominant Wave Number, k_o	0.0716 radian/m
Equilibrium Coefficient, β	0.0048
Mean Square Surface Slope, $\overline{(\nabla\zeta)^2}$	0.01406 radian^2
Significant Wave Height, $4(\overline{\zeta^2})^{\frac{1}{2}}$	2.94 m

The shortest wave length used in the evaluation of $\overline{(\nabla\zeta)^2}$ for Table 4.1 is 0.3 m. as cited by Cox and Munk (1954). For $k>k_o$, by the method of the least square fitting, a linear relationship can be established on the basis of equilibrium range by Phillips (1958) as

$$\log S(k) \underset{k>k_o}{} = - 1.0913 \log k - 2.6036 \qquad (4.1)$$

where S(k) is the wave number slope spectrum. The mathematical slope of -1.0913 in Equation (4.1) between log $S(k)_{k>k_o}$ and log k is in remarkable agreement with that theoretically predicted by Phillips (1969). Phillips' theoretical value of this slope is -1.

V. DIRECTIONAL WAVE NUMBER SLOPE SPECTRUM

Guided by basic theoretical understandings (Phillips, 1969; Chen, 1972) the directional wave number slope spectrum, $s(k,\alpha)$, is generally defined and written as the product of a wave number dependent function, $S'(k)$, and a wave number dependent angular spreading function $H(k,\alpha)$ as

$$s(k,\alpha) = S'(k)H(k,\alpha) \qquad (5.1)$$

where the directional parameter, α, is measured with reference to the direction of the average wind. As detailed in Chen (1972) this form has been suggested by many investigators, but insufficient data exists to specify $H(k,\alpha)$. More than often a simplified version of $H(k,\alpha)$, $H'(\alpha)$, is used. In other words, this simplified version assumes that the angular spreading function is only the function of the directional parameter α, or from Equation (5.1),

$$s(k,\alpha) = S'(k)H'(\alpha). \qquad (5.2)$$

It is further assumed that wave energy should be symmetrically distributed about the mean wind vector. Therefore $H'(\alpha)$ is an even function of α and, in particular, is

chosen to be an even function of cosine function or functions,

$$H'(\alpha) = \sum_J B_J(J) \cos^{2J} \alpha \tag{5.3}$$

where J is an integer and

$$\int_{-\pi/2}^{\pi/2} [\sum_J B_J (J) \cos^{2J}\alpha] d\alpha = 1 \tag{5.4}$$

In the absence of the summation operator in Equation (5.4) $H'(\alpha)$ assumes the forms of

$$H'(\alpha) = \begin{cases} 1/\pi & J=0 \\ (2/\pi)\cos^2\alpha & J=1 \\ (8/3\pi)\cos^4\alpha & J=2 \\ (16/5\pi)\cos^6\alpha & J=3 \\ (128/35\pi)\cos^8\alpha & J=4 \\ (256/63\pi)\cos^{10}\alpha & J=5 \end{cases} \tag{5.5}$$

Furthermore, the relationship between S(k) and S'(k) can be readily established to be

$$S'(k) = S(k)/k \tag{5.6}$$

by definition,

$$\int_k S(k)dk = \int_k [\int_\alpha s(k,\alpha)k d\alpha] dk \tag{5.7}$$

and Equations (5.2), (5.3), and (5.4).

Therefore, from Equations (5.2), (5.3), and (5.6), a relationship between the directional wave number slope spectrum $s(k,\alpha)$ and wave number slope spectrum S(k) is

$$s(k,\alpha) = \frac{S(k)}{k} \sum_J B_J(J) \cos^{2J}\alpha \tag{5.8}$$

or

$$\log \underset{k>k_o}{s(k,\alpha)} = \log \underset{k>k_o}{S(k)} - \log k + \log\left[\sum_J B_J(J)\cos^{2J}\alpha\right]. \quad (5.9)$$

From Equations (4.1) and (5.9) it is quite obvious to establish,

$$\log \underset{k>k_o}{s(k,\alpha)} = -2.0913 \log k - 2.6036 + \log\left[\sum_J B_J(J)\cos^{2J}\alpha\right]. \quad (5.10)$$

It is also important to notice that the assumptions made in Equations (5.2) and (5.3) are for the wind-generated waves. Swells have anisotropic angular distributions which approach those of waves generated by strong winds. Nevertheless, the existence of swells, which distort the angular distribution in a narrow band-width, should be detectable by the measurements. However, instruments like the laser profilometer cannot provide the capability of resolving the term $\sum_J B_J(J)\cos^{2J}\alpha$ (McClain, et al, 1978).

By an educated guess, based upon the ground truth information presented in Section 4 and the report by McClain, et al. (1978), it is logical to assume that the angular spreading function $\sum_J B_J(J)\cos^{2J}\alpha$ has the form of

$$\sum_J B_J(J)\cos^{2J}\alpha = B_0(0) + B_1(1)\cos^2\alpha + B_2(2)\cos^4\alpha. \quad (5.11)$$

This is a very realistic assumption because, except for extraordinary circumstances of the existence of very large swells, Equation (5.11) is adequate for the wind-generated gravity waves in ocean (Cote, et al, 1960; Pierson, 1969 and 1970). Swells will appear as a peak generally in the region of $k<k_o$ and can be readily observed. For the

general application, an extra term of $B_3(3)\cos^6(\alpha-\alpha_s)$ or $B_4(4)\cos^8(\alpha-\alpha_s)$ can be added to Equation (5.11), where α_s is the orientation of the swell with respect to wind direction.

VI. RESULT

Figures 3.2 and 6.1 are the antenna patterns for files 0 and 1, respectively, These two files were taken while the aircraft was flying across the wind. Thus, the horns were pointed along the wind direction. Although there is scatter from the mean trends of these two figures, this scatter is quite similar in relative magnitudes and range locations. Because of the random nature of this scatter, the similarities between these figures are quite striking. The scatter is definitely due to the short duration of 2.84 seconds for averaging. Yet, the similarities demonstrate the homogeneity of the ocean surface because files 0 and 1 are at least ten kilometers apart in physical locations. Furthermore, the mean trends shown in Figures 3.2 and 6.1 exhibit the expected radar antenna pattern.

Ocean wave slopes as functions of horizontal distances for a typical sweep of files 0 and 1 are shown in Figures 3.3 and 6.2, respectively. These wave slopes have the maximum value of under 0.03 radians which is much less than the theoretical limit of 0.0505 radians derived by Stoker (1957). These figures show wave slope spikes with spatial width of the order of 10 meters and above. This order of magnitude is indeed larger than what is desired.

The directional wave number slope spectra for file 0 and 1 are shown in Figures 3.4 and 6.3, respectively. Each spectrum is derived with 7936 degrees of freedom. These two wave number slope spectra are almost identical. Nevertheless, there are no apparent spectral peak at k_o (0.0716 radian/m) as shown in Table 4.1. This undesirable

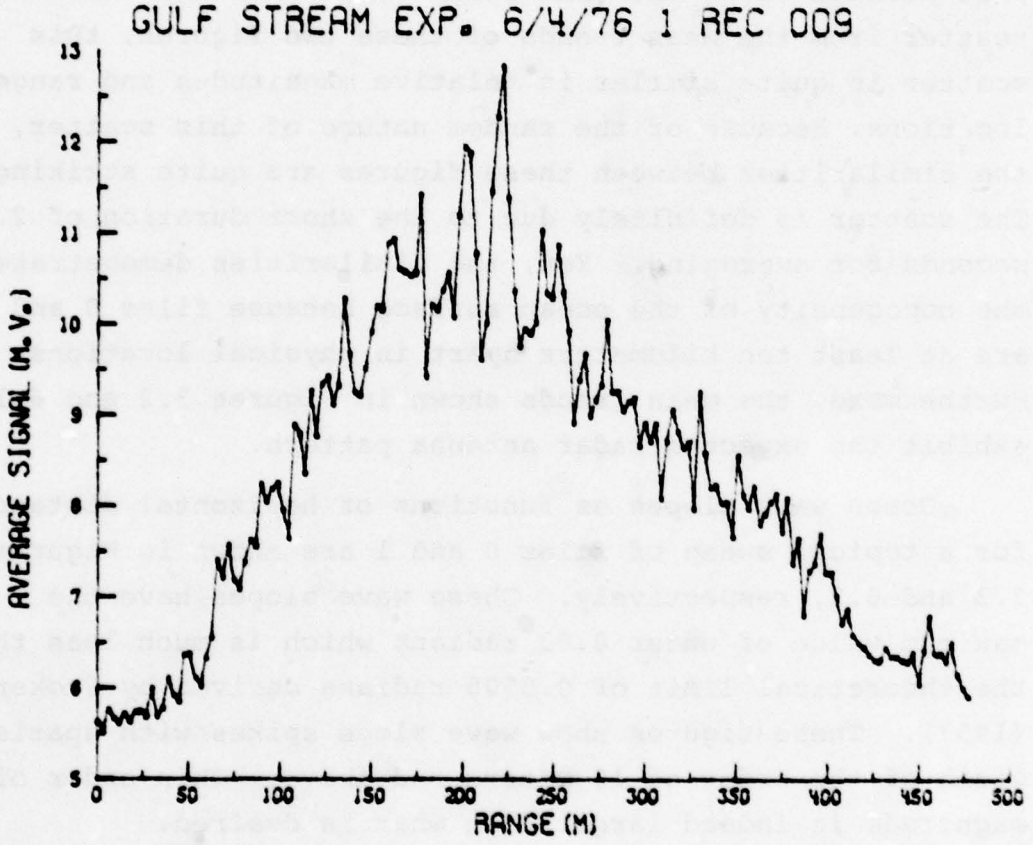

Fig. 6.1 - Antenna pattern

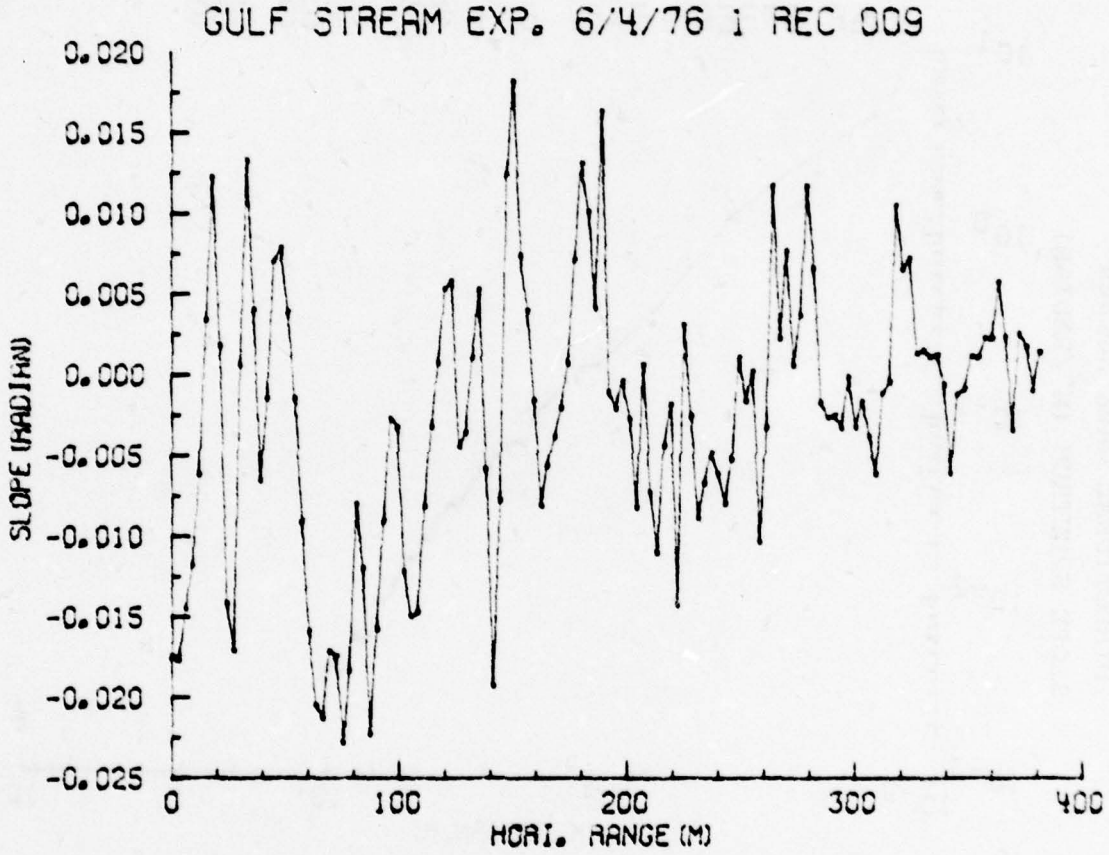

Fig. 6.2 - Local wave slope

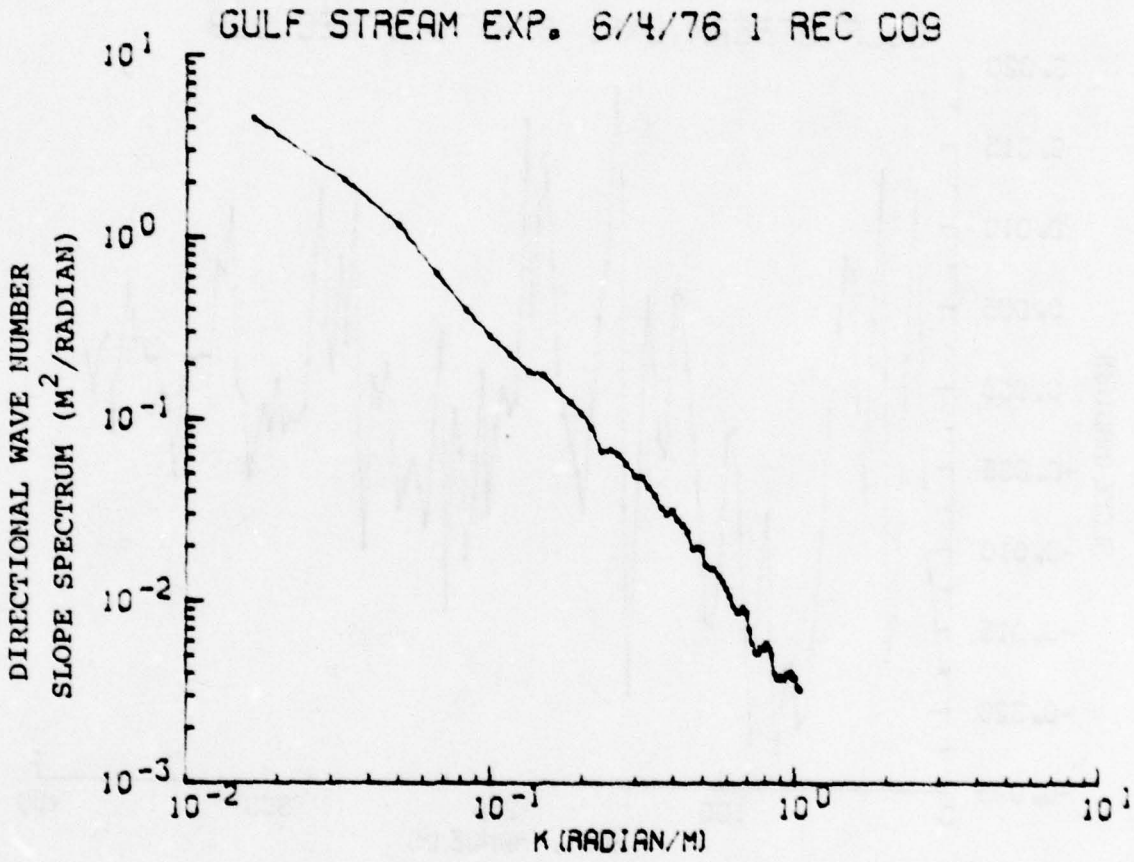

Fig. 6.3 - Directional wave number slope spectrum

characteristic may well be caused by both the short spatial segment of less than 400 meters as shown by Figure 3.3 or 6.2, and the coarse spatial resolution. Through data fitting technique, Figures 3.4 and 6.3 can be represented for $k>k_o$, by

$$\log s_{w_{k>k_o}}(k,0) = -1.8691 \log k - 2.3991 \qquad (6.1)$$

where $s_w(k,0)$ is the directional wave number slope spectrum derived from the ocean wave spectrometer. The value of the mean square surface slope $\overline{(\nabla\zeta)^2}$ used in deriving Equation (6.1) is 0.01406 radian^2 as shown in Table 4.1 by the ground truth. Whereas, by using Equation (2.18) for $\overline{(\nabla\zeta)^2}$ as proposed by Cox and Munk (1954) the mean square surface slope $\overline{(\nabla\zeta)^2}$ assumes the value of 0.0414 radian^2 for wind speed of 7.5 m/s and the derived directional wave number slope spectra for files 0 and 1 are shown in Figures 6.4 and 6.5, respectively.

By comparing Figures 6.4 with 3.4 and Figures 6.5 with 6.3 one can see very little difference between them except the ordinates have been shifted linearly upward for Figures 6.4 and 6.5. There are several observations which can be made on the consequences of using different values of $\overline{(\nabla\zeta)^2}$ for analysis of the same set of ocean wave spectrometer data:

1. The inferred value of $\overline{(\nabla\zeta)^2}$ by Cox and Munk (1954) is about 3 times larger than the value of $\overline{(\nabla\zeta)^2}$ measured by ground truth. A larger value of $\overline{(\nabla\zeta)^2}$ scatters more electromagnetic energy away from the receiving horn and, thus, gives less return power. In order to maintain the same level of return power, by looking at the mathematical model of Equation (2.17), the inferred local wave slope

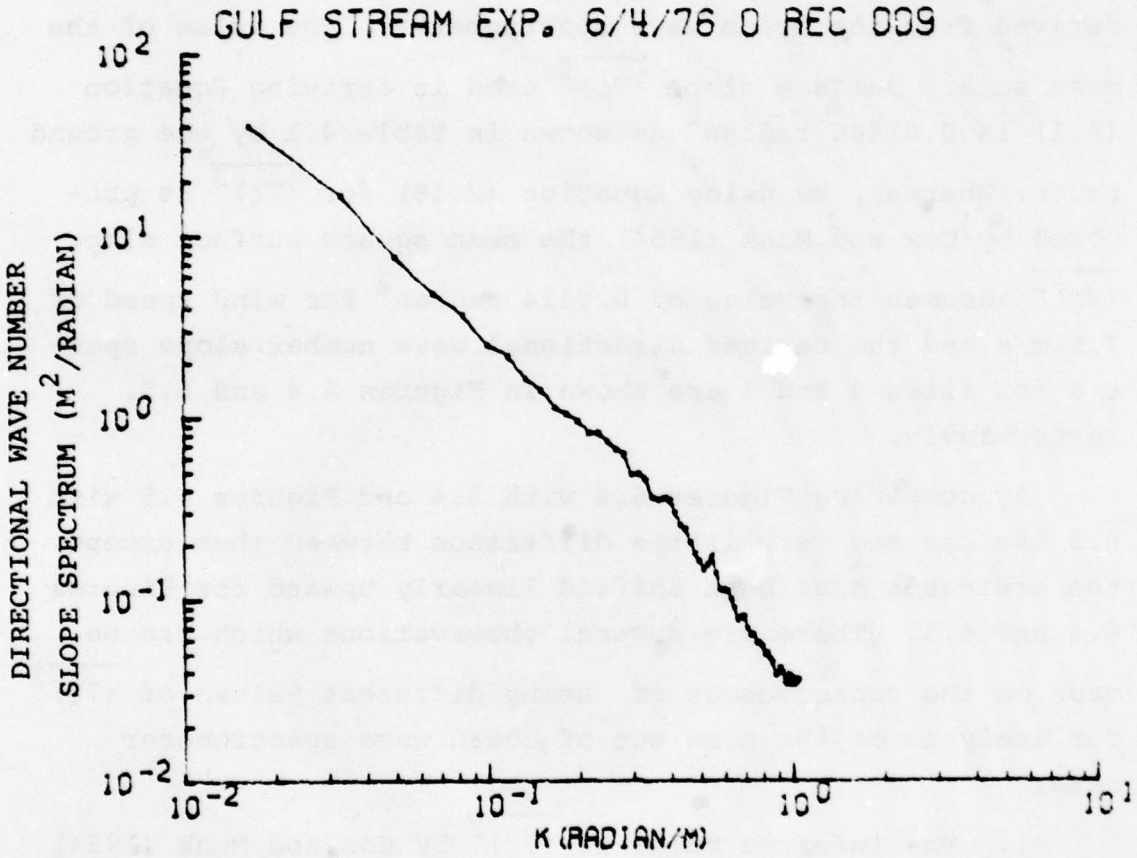

Fig. 6.4 - Direction wave number slope spectrum

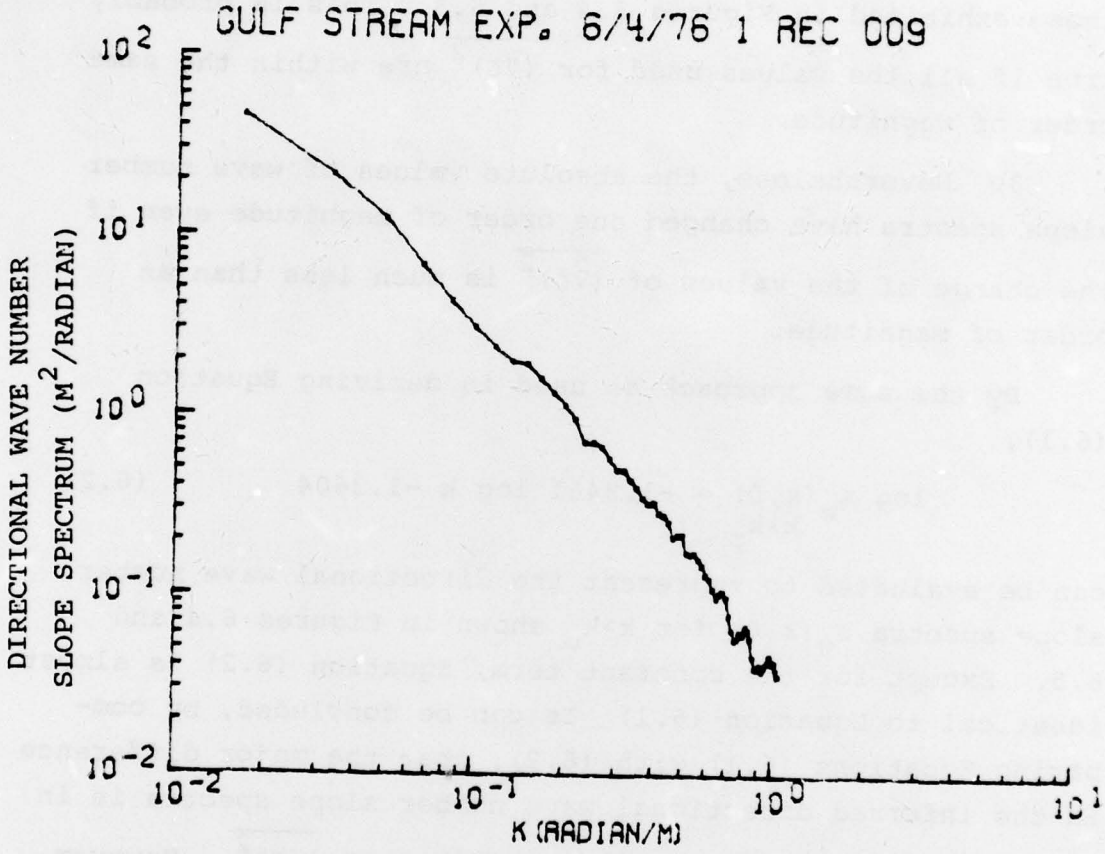

Fig. 6.5 - Directional wave number slope spectrum

$\tan\kappa$ has to be increased.

2. For small value of κ, say $\kappa \ll 1$, $\tan\kappa \doteq \kappa$ in Equations (2.19) and (2.20). In other words, a linear relationship exists for the tangent function for the small κ. It is, thus, very obvious that the mathematical curve slopes of the directional wave number slope spectra in Figures 6.4 and 6.5 do not have the noticeable change from those exhibited in Figures 3.4 and 6.3. This is probably true if all the values used for $\overline{(\nabla\zeta)^2}$ are within the same order of magnitude.

3. Nevertheless, the absolute values of wave number slope spectra have changed one order of magnitude even if the change of the values of $\overline{(\nabla\zeta)^2}$ is much less than an order of magnitude.

By the same approach as used in deriving Equation (6.1),

$$\log s_w(k,0)_{k>k_o} = -1.8461 \log k - 1.3604 \qquad (6.2)$$

can be evaluated to represent the directional wave number slope spectra $s_w(k,0)$ for $k>k_o$ shown in Figures 6.4 and 6.5. Except for the constant term, Equation (6.2) is almost identical to Equation (6.1) It can be concluded, by comparing Equations (6.1) with (6.2), that the major difference in the inferred directional wave number slope spectra is in the constant terms for different values of $\overline{(\nabla\zeta)^2}$. However, this constant term determines the absolute values of the amplitude of the inferred directional wave number slope spectra. Therefore, the value of $\overline{(\nabla\zeta)^2}$ used is very important to the eventual output of the ocean wave spectrometer. This conclusion points to the requirement for

measuring the mean square surface slope $\overline{(\nabla\zeta)^2}$ by independent means.

By comparing the directional wave number slope spectrum $s_w(k,0)$, which is inferred by the ocean wave spectrometer, in Equation (6.1) with that provided by the ground truth, $s(k,0)$, in Equation (5.10) for $k>k_o$ it can be concluded that,

$$\log \underset{k>k_o}{s(k,0)} = \log \underset{k>k_o}{s_w(k,0)} - 0.2222 \log k, \qquad (6.3)$$

and

$$\log[\sum_J B_J(J)] = 0.2045 - C\,. \qquad (6.4)$$

The second term on the right hand side of Equation (6.3) has a coefficient of -0.2222, instead of a desired "0.". There are probably three explanations for this term:

1. The beam width of ocean wave spectrometer is larger than that of the laser profilometer so that the automatic averaging over the beam width of the ocean wave spectrometer has been included in the data.

2. The wind effects, through the mean square surface slope, would redistribute the energy contained in the longer waves to the shorter waves so that a larger value of the mean square surface slope would make the curve $\log \underset{k>k_o}{s_w(k,\alpha)}$ with $\log k$ flatter. This tendency has been demonstrated in Equations (6.1) and (6.2).

3. The angular spreading functions, $H(k,\alpha)$, should be a function of wave number, k, albeit this dependency may be weak and, also, nonuniform.

However, it is believed that the first two reasons are predominant because the directional wave number slope spectrum given by Equation (6.1) of the ocean wave

spectrometer agrees very well with those inferred by Valenzuela, et al (1971) from their airborne Doppler radar measurements. Their results show the same conclusions.

As to Equation (6.4), the term C is the summation of biases and noises. In the absence of the summation sign in Equation (6.4) and, also, with the values of $\hat{B}_J(J)$ provided by Equation (5.5)

$$\log \hat{B}_0(0) = -0.497, \quad \log \hat{B}_1(1) = -0.196,$$
$$\log \hat{B}_2(2) = -0.071, \quad \log \hat{B}_3(3) = 0.008,$$
$$\log \hat{B}_4(4) = 0.066, \quad \log \hat{B}_5(5) = 0.112,$$

where the "$\hat{}$" sign denotes no summation. In light of these values, Equation (6.4) should assume the form of

$$\log[\sum_{J>7} B_J(J)] = 0.2045 \tag{6.5}$$

if C = 0. We have learned, from the ground truth, in Section 4 and definitions in Section 5, that Equation (6.5) just cannot be true. Therefore, a nonzero positive C should be included in Equation (6.4) by simple logic of deduction. Furthermore, the term C can be defined, in general, to be

$$C = C_z + C_s + C_{sl} + C_{fs} + C_B \tag{6.6}$$

where

1. C_z is zero-set noise in the ocean wave spectrometer. his noise is believed to be very small because the data has been zero-set by the software. This term is, nevertheless, positive.

2. C_s is the nonlinear scale noise in the ocean wave spectrometer. This noise is, also, believed to be very small because the system has been monitored very carefully during the experiment. This term can be either positive or

negative in value.

3. C_{sl} is the energy leakage noise caused by the side-lobes of the digital delta function. This term is very small and, also, negative in nature.

4. C_{fs} is the noise caused by the existence of foam and spray on the ocean surface. The term has a large positive number in value. However, this noise can be removed by thorough and systematic calibration measurements against passive microwave remote sensing or in-situ measurements. This was not planned in the Gulf Stream Experiment.

5. C_B is the noise caused by the Bragg scattering at the electromagnetic frequency of 9.75 GHz in the large nadir looking angles with respect to the local wave slopes. The removal of this type of noise required the techniques of polarized composite analysis. The polarized measurement was not made in this experiment. C_B can assume a moderate positive value.

Therefore, the terms included in C can be classified into two categories. The first category of terms which include C_z, C_s, and C_{sl} is those terms associated with the system. This first type of noise can only be reduced to the bias level. The second category of terms which include C_{fs} and C_B is those terms associated with the analyses. The removal of the major part of this second type of noise would require additional thorough and systematic calibration measurements against well-instrumented test areas.

Referring back to Equations (5.4), (5.5), and (5.11) it is quite obvious that Equation (5.11) has the values from $\hat{B}_0(0)$ to $\hat{B}_2(2)$ for $\alpha=0^\circ$ in which the symbol "$\hat{}$" denotes no summation, $\hat{B}_0(0) = 1/\pi$, and $\hat{B}_2(2) = 8/3\pi$. As a consequence, from Equations (5.11) and (6.4),

$$\log(1/\pi) = 0.2045 - C, \qquad (6.7)$$

and

$$\log(8/3\pi) = 0.2045 - C\ . \qquad (6.8)$$

Equation (6.7) gives the value of C an upper bound at 0.7045 whereas Equation (6.8) gives the value of C a lower bound at 0.2755. This is to say, equivalently, that $s_w(k,\alpha)$ should be divided by a number with the value from $10^{0.2755}$ to $10^{0.7045}$ so that the total noise and bias can be removed. Unfortunately, the value of this number cannot be pinpointed because the Gulf Stream Experiment lacked the complicated and precise ground truth arrangements required.

Assuming the value of C is constant over the directional measurements, the range J of the summation and the values of the $B_J(J)$s can be determined by J independent directional measurements. In the case the six-leg measurements shown in Figure 4.1 only three directional measurements are independent because statistical methods have been used in evaluating the spectra. These methods have 180° ambiguities which make those directional measurements at $\alpha = 0^\circ$, $\alpha = 45^\circ$, and $\alpha = 90^\circ$ the independent measurements. Therefore only three $B_J(J)$s can be assumed and evaluated by these independent measurements.

For the general application when the existence of swells is observed, an extra term of $B_3(3)\cos^6(\alpha-\alpha_s)$ or $B_4(4)\cos^8(\alpha-\alpha_s)$ can be added to Equation (5.11), where α_s is the orientation of the swell, and four, instead of three, independent directional measurements would be required to resolve the $B_J(J)$s if α_s is known.

In the Gulf Stream Experiments three independent directional measurements were made which is adequate to solve for $B_0(0)$, $B_1(1)$, and $B_2(2)$ in Equation (6.7) by using Equation (6.4) two more times for $\alpha=45^\circ$ and $\alpha=90^\circ$.

Unfortunately, the undesirably large spatial resolution of the measurements renders the results meaningless for $\alpha=45^{o}$ and $\alpha=90^{o}$. Nevertheless, the systematic ingredients for resolving the directional wave number slope spectrum by the ocean wave spectrometer are there.

VII. DISCUSSION

1. Due to the wave-wave interactions (Phillips, 1960; Longuet-Higgins, 1962), short waves are continuously taking energy away from the long waves and, subsequently, this energy is dissipated through breaking and viscous damping. But, also, these short waves on the sloping faces of the long wave behind the crests (or windward faces if the long wave is propagating in the same direction as the wind) are extended or stretched and those short waves on the sloping faces of the long wave in front of the crests (or leeward faces) are compressed. These types of second order oceanic dynamic processes not only boost the value of local mean square surface slopes for the sloping faces in front of the crests, but also decrease the value of local mean square surface slopes of the sloping faces behind the crests. By using Equation (2.17), the specular point model, the inferred local wave slopes are artificially increased and decreased accordingly. These evaluations of local wave slopes result in distorted wave slope profiles. Through spectral analysis the energy contained in the long waves is to be aliased to waves with higher wave numbers. In other words the slope of log $s_{w}(k,\alpha)_{k>k_{o}}$ with log k is flattened from what is expected otherwise.

2. The required modification of the Fresnel reflection coefficient for angles away from normal incidence cited by Valenzuela (1976) is not necessary because the averaging process is applied to each individual radar local look-angle

and, subsequently, the resultant is normalized.

3. In evaluating $\overline{(\nabla\zeta)^2}$ from the ground truth, only the mean square surface slopes contributed by ocean waves which are long in comparison to the wavelength of the electromagnetic waves are included.

4. The inclusion of the composite surface scattering model (Brown and Miller, 1977; Wright, 1968) which requires polarized measurements of radar cross section at large look-angles from the nadir is not fully justified for this experiment because the local look-angles used are less than 20^{o} from the nadir. The inclusion of polarized measurements in the future experiments is, nevertheless, necessary to test some of the theoretical predictions of Bragg scattering if a better instrument is desired.

VIII. CONCLUSION AND RECOMMENDATION

The ocean wave spectrometer has been proved to be capable of providing the directional wave number slope spectra. Based upon definition, these directional wave number slope spectra can be converted to the directional wave number spectra, through division by k^2, if it is so desired.

It is advantageous to have a summary table which includes assumptions and required measurements for the ocean wave spectrometer in its measurement of directional wave number slope spectra:

SUMMARY TABLE

Assumptions:

Statistically stationary and homogeneous ocean surface; radius of curvature of the ocean surface is much larger than the electromagnetic wavelength, i.e., $\rho >> \lambda$ given by Equation (2.14); the absolute value of the slope of

ocean surface is less than one, i.e., $|\nabla\zeta|<1$ given by Equation (2.15); $\overline{(\zeta^2)}^{\frac{1}{2}} \cos\theta >> \lambda$ given by Equation (2.16); finite conducting ocean surface; Gaussian-distributed ocean surface; angular spreading function is only the function of the directional parameter α as given in Equation (5.2); wave energy is symmetrically distributed about the mean wind vector.

Measurements Required:

Precision altitude measurement; precision tilt angle measurement with the local vertical; independent measurement of the mean square surface slope, $\overline{(\nabla\zeta)^2}$; Four independent directional measurements, in reference to the known wind direction, by ocean wave spectrometer; the measurement of the direction of wind; independent measurement of foam and spray; look-angle is less than 20°.

Nevertheless, recommendation for further studies on the ocean wave spectrometer is required. These studies include:

1. Study of the effects due to foam and spray on the measurements, i.e., the term C_{fs} in Equation (6.6) against well-instrumented test area for wind, foam and spray, and directional wave number spectra, and

2. Study of the statistical error contained in the terms $B_J(J)$s in Equation (5.3) against the same test area.

It is quite obvious that a better spatial resolution, say 0.1 meter or smaller, and a larger spatial coverage, say between 750 meters and 1000 meters, are necessary.

ACKNOWLEDGEMENT

The principal author would like to thank Mr. B.S. Yaplee and Dr. V.E. Noble for their support and encouragement during the course of this study. We are also indebted to Mr. J.T. McGoogan and Dr. N.E. Huang of NASA Wallops Flight Center for their assistances and permission to use their C-54 for this particular experiment. Thanks are also dued to Mrs. M. Thompson for her typing and Mrs. J. Ware for her drawing.

The funds for this report are provided by NAVAIR Task No. A370/370C/058B/WF52-553000 to NRL, and NRL 6.1 Task Area RR-031-03-43 Program Element 61153N-31.

REFERENCES

Barrick, D.E., Rough Surface Scattering Based on the Specular Point Theory, IEE Transactions, Antennas and Propagation, Vol. AP-16, 449-454, 1968

Blackman, R.B., and Tukey, J.W., The Measurement of Power Spectra, Dover Publications, Inc., New York, 1958

Brooks, L.W., and Dooley, R.P., Technical Guidance and Analytical Services in Support of SEASAT-A, NASA CR-141399, 1974

Brown, G.S., and Miller, L.S., Microwave Backscattering Theory and Active Remote Sensing of the Ocean Surface, NASA Wallops Flight Center Report CR-141423, 1977

Chen, D.T., The Directional Fetch-Limited Spectra for Wind-Generated Waves, Ph.D. Thesis, North Carolina State University, 1972

Chen, D.T., Definition of Directional Wave Spectral Measurement Requirements for Active Microwave Sensors of Remote Ocean Surface Measuring System (ROMS), Memorandum Report 3818, the Naval Research Laboratory, 1978

Cote, L.J., Davis, J.O., Marks, W., McGough, R.J., Mehr, E., Pierson, W.J., Jr., Ropek, J.F., Stephenson, G., and Vetter, R.C., The Directional Spectrum of a Wind-Generated Sea as Determined from Data Obtained by the Stereo Wave Observation Project, New York University, College of Engineering, Meteorology Papers, 2(6), 1960.

Cox, C.S., and Munk, W., Measurement of the Roughness of the Sea Surface from Photographs of the Sun's Glitter, Journal of the Optical Society of America, Vol. 44, 838-850, 1954

Eckerman, J., and Hammond, D.L., Radar Observation of Ocean Wave Slope Spectra, IEEE/URSI Symposium, Atlanta, 1974

Hagfors, T., Backscattering from an Undulating Surface with Applications to Radar Returns from the Moon, Journal of Geophysical Research, Vol. 69, 3779-3784, 1964

Hammond, D.L., Mennella, R.A., and Walsh, E.J., Short Pulse Radar Used to Measure Sea Surface Wind Speed and SWH, IEEE Transactions, Antennas and Propagation, Vol. AP-25, No. 1, 61-67, 1977

Le Vine, D.M., Walton, W.T., Eckerman, J., Kutz, R.L., Dombrowski, M., and Kalshoven, J.E., Jr., GSFC Short Pulse Radar, JONSWAP-75, NASA TN D-8502, 1977a

Le Vine, D.M., Davisson, L.D., and Kutz, R.L., Monte Carlo Simulation of Wave Sensing with a Short Pulse Radar, NASA/GSFC X-953-77-239, 1977b

Longuet-Higgins, M.S., Resonant Interactions between Two Trains of Gravity Waves, Journal of Fluid Mechanic, Vol. 12, 321-332, 1962

McClain, C.R., Chen, D.T., and Hammond, D.L., Gulf Stream Ground Truth Project: Results of NRL Airborne Sensors, Memorandum Report 3779, The Naval Research Laboratory, 1978

Myers, G.F., High Resolution Radar Part IV - Sea Clutter Analysis, Report 5191, The Naval Research Laboratory, 1958

Phillips, O.M., The Equilibrium Range in the Spectrum of Wind-Generated Waves, Journal of Fluid Mechanics, Vol. 4, 426-434, 1958

Phillips, O.M., On the Dynamics of Unsteady Gravity Waves of Finite Amplitude, Part 1 The Elementary Interactions, Journal of Fluid Mechanics, Vol. 9, 193-217, 1960

Phillips, O.M., The Dynamics of the Upper Ocean, Cambridge University Press, 1969

Pierson, W.J., Jr., A Proposed Vector Wave Number Spectrum for the Study of Radar Sea Return, Microwave Observations of the Ocean Surface, SP-152, U.S. Oceanographic Office, 251-292, 1969

Pierson, W.J., Jr., A Proposed Vector Wave Number Spectrum for the Study of Radar Sea Return, New York University, Department of Meteorology and Oceanography, Geophysical Science Laboratory Contribution, 87, 1970

Schooley, A.H., Upwind-Downwind Ratio of Radar Return Calculated from Facet Size Statistics of a Wind-Disturbed Water Surface, Proceedings, Institute of Radio Engineers, Vol. 50, 456-461, 1962

SEASAT-A Scientific Contributions, National Aeronautics and Space Administration, 1974

Skolnik, M.I., Radar Handbook, McGraw-Hill, New York, 1970

Stoker, J.J., Water Waves, Interscience Publishers, Inc., New York, 1957

Tomiyasu, K., Short Pulse Wide-Band Scatterometer Ocean Surface Signature, IEEE Transactions, Geoscience Electronics, Vol. GE-9, No. 3, 175-177, 1971

Walsh, E.J., Analysis of Experimental NRL Radar Altimeter Data, Radio Science, Vol. 9 (Nos. 8 and 9), 711-722, 1974

Wright, J.W., A New Model for Sea Clutter, IEEE Transactions Antennas and Propagation, Vol. AP-16, 17281729, 1968

Yaplee, B.S., Shapiro, A., Hammond, D.L., and Uliana, E.A., Ocean Wave Height Measurements with a Nanosecond Radar, Proceedings, 7th International Symposium on Remote

Sensing of Environment, The University of Michigan, 1879-1893, 1971

Zamarayev, B.D., and Kalmaykov, A.L., On the Possibility of Determining the Spatial Structure of an Agitated Ocean Surface by Means of Radars, Izv, Atmospheric and Ocean Physics, Vol. 5, No. 1, 124-127, 1969

Valenzuela, G.R., Laing, M.B., and Daley, J.C., Ocean Spectra for the High Frequency Waves as Determined from Airborne Radar Measurements, Journal of Marine Research, Vol. 29, 69-84, 1971

Valenzuela, G.R., Intersection of Electromagnetic and Oceanic Waves - A Review, IUCRM Colloquium on Radio Oceanography, Sept. 29 to Oct. 6, 1976, Hamburg, W. Germany